Egypt. J. Chem. **Vol. 67**, No. 5. pp. 77- 88 (2024)

Egyptian Journal of Chemistry

http://ejchem.journals.ekb.eg/

A Comparative Determination of Chromotrope 2R Dye through Colorimetric and Fluorimetric Detection after Solid Phase Microextraction Using Spinel $NiFe_2O_4$

Samer S. Aburub[a], Nurul Y. Rahim*[a], Ashraf M. Mahmoud[b]

[a] *School of Chemical Sciences, Universiti Sains Malaysia, 11800, Pulau Pinang, Malaysia*

[b]*Department of Pharmaceutical Chemistry, College of Pharmacy, Najran University, Najran, Saudi Arabia*

Abstract

In this study, a facile, convenient, and cost-effective vortex-assisted dispersive solid phase microextraction (VA-D-µ-SPE) was proposed to pre-concentrate chromotrope 2R dye (C2R) from watery media. Nickel ferrite nanoparticles ($NiFe_2O_4$ NPs) were used as an efficient sorbent for C2R, while colorimetric and fluorimetric methods were used to quantify C2R. The colorimetric method is based on measuring the native color of C2R at λmax 510 nm, while fluorescence sensing is based on quenching the fluorescence emission of red-emissive cationic carbon dots (rcCDs) at λem 680 nm via the electrostatic interaction and inner-filter effect (IFE). Factors affecting VA-D-µ-SPE and the determination were carefully optimized. Characterization of $NiFe_2O_4$ NPs and rcCDs was confirmed by scanning electron microscopy (SEM), transmission electron microscopy (TEM), energy dispersive X-ray (EDX), fourier transform infrared spectroscopy (FT-IR), powder X-ray diffraction (PXRD), thermogravimetric analysis (TGA), vibrating sample magnetometer (VSM), UV/Vis spectroscopy, and fluorescence spectroscopy. The as-fabricated rcCDs exhibited a fluorescence quantum yield of 24.4%. It was found that the absorption intensities were increased linearly with increasing C2R concentration in the range of 10–60 µM with a detection limit (S/N = 3) of 3.1 µM, while the fluorescence intensities were decreased linearly in the range of 5–50 µM with a detection limit (S/N = 3) of 1.6 µM. The adsorption isotherm was best fitted to the Freundlich model with an R^2 value of 0.9958 and a maximum adsorption capacity (q_m) value of 151.5 $mg.g^{-1}$. Adsorption kinetics was described by a pseudo-second-order model with R^2 of 0.9962. Importantly, the VA-D-µ-SPE was successfully applied to determine C2R in water and tap water samples with acceptable percentage recoveries in the range of 92.6–102.4% and RSD % not more than 3.5%, suggesting the reliability of the proposed methods.

***Keyword*:** Chromotrope 2R dye (C2R); Red-emissive cationic carbon-dots (rcCDs); Nickel ferrite nanoparticles ($NiFe_2O_4$ NPs); Colorimetry; Fluorometry.

1- Introduction

Nowadays, huge amounts of commercially available industrial dyes are produced annually [1]. Dyes are classified into cationic dyes or anionic dyes according to their composition and structure [2-5]. Dyes are stable to light, heat and oxidizing agents owing to their aromatic structures [6]. They are considered one of the most dangerous pollutants to the aquatic environment because they give unacceptable colour and decrease the penetration of sunlight into the aquatic environment [7-11]. Dyes are used in many industries, such as textiles, wool, nylon, and canned foods. Due to the expensive costs of natural food dyes and their damage during processing or storage, artificial dyes are usually used as colouring agents in food industries [12, 13]. Dyes pose a high risk to human health in cases of misuse [13, 14]. Chromotrope 2R dye (C2R), shown in Scheme 1, is an anionic red azo-dye used in different fields such as: paper, leather, and textile industries, as well as some cosmetics [15]. It is a carcinogenic dye that is hydrolyzed to aromatic amines and sulphanilic acid [16]. Moreover, it causes respiratory irritation and skin inflammation [17]. It is reported that the maximum residual limit of C2R in the wastewater is ranged from 10 to 200 $mg.L^{-1}$ [17]. Spectroflourimetry and UV-VIS spectrophotometry have been used to analyze various environmental samples owing to their simplicity, affordability, and wide availability in most research laboratories.

*Corresponding author e-mail: nurulyanirahim@usm.my

Receive Date: 29 September 2023, Revise Date: 22 October 2023, Accept Date: 06 November 2023

DOI: 10.21608/EJCHEM.2023.239597.8691

Additionally, the real environmental samples are complex matrices that contain low dye concentrations. As a result, they require separation coupled with a pre-concentration method to concentrate, isolate, and extract dye from their complex matrices, which leads to advancement of the analytical selectivity and sensitivity. Literature survey revealed that C2R dye was removed from aqueous samples using activated carbon via colorimetric detection [15] and mesoporous carbons modified with lanthanum [18]. Industrial demands have generated a growing need for nanomaterials, especially with desirable particle sizes and shapes for a variety of applications [19-21]. The nanomaterials inherently have large surface areas and improved mechanical and catalytic properties [22, 23]. Enhancement of the chemical, magnetic, optical, and surface properties of the nanoparticles has been attributed to their unique quantum size, which makes them applicable in catalysis, biomarkers, biosensors, colour imaging, and pigments [20, 24]. Recently, nanoparticles have emerged as dye adsorbents [25]. Previous reports explained that the efficacy and capacity of the adsorbent materials depend on their surface area, large number of active sites, and porosity distribution [25]. Therefore, nanoparticles may be considered one of the most powerful adsorbent for vortex-assisted dispersive solid-phase microextraction (VA-D-μ-SPE) for dye removal from aqueous media [26]. VA-D-μ-SPE is a low-cost, simple, and quick method for extracting target molecules as well as cleaning up real-world samples with a high enrichment factor and low sample volume consumption [26-28]. Among the diverse nanomaterials, binary metal oxides with various configurations have attracted growing industrial and technical concern owing to their magnetic properties. Magnetic nanoparticles have gained great attention in the adsorption of various analytes due to their ease of dispersion and separation from solutions using an external magnet. Spinel $NiFe_2O_4$ nanoparticles ($NiFe_2O_4$ NPs) are a well-known model of magnetic nanoparticles that have been used in many applications such as catalysis, biosensors, and adsorbents. They have many advantages, including high chemical and thermal stability, good adsorption efficiency, and fast phase separation [26, 29]. The magnetic behaviour of $NiFe_2O_4$ NPs depends on their size and geometry [29, 30]. Carbon dots (CDs) have been hailed as a potential substitute for traditional dyes due to their many advantages, such as water dispersion, affordability, luminescence properties, and low toxicity [31-36]. The hydrothermal method is the most commonly used approach for the fabrication of CDs due to its low-cost and short fabrication time [37, 38].

In this work, a simple VA-D-μ-SPE using dual-mode detection for the sensitive and selective determination of C2R dye in watery media was proposed. The method is based on extracting C2R dye using spinel $NiFe_2O_4$ NP as an adsorbent, followed by colorimetric and fluorometric determinations.

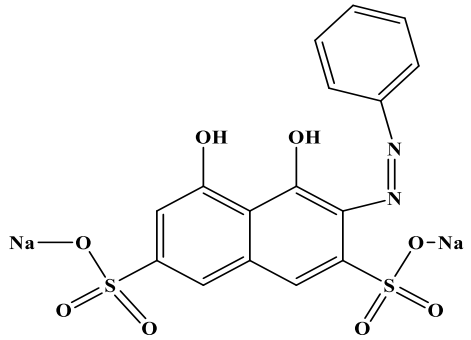

Scheme 1: Chemical structure of chromotrope 2R (C2R).

2. Experimental

Materials, reagents, instrumentations, evaluation of adsorption isotherms on C2R dye, and determination of the quantum yield (Φs) of the rcCDs have been discussed in detail in the Electronic Supplementary Materials (ESM).

2.1. Synthesis of nickel ferrite nanoparticles ($NiFe_2O_4$ NPs)

The synthesis of $NiFe_2O_4$ NPs followed the previous report with some modifications [39]. 3.0 g of $FeCl_3.6H_2O$ (dissolved in 50 mL of 0.5 M HCl) and 0.5 g $NiSO_4.7H_2O$ were solubilized in 500 mL 0.5 M NaOH and sonicated for 30 min. Then, 3.0 g of urea was added to the suspension and vigorously stirred for 45 min. The suspension was autoclaved for 12 hrs at 200 °C. The product was then separated using a magnet, washed several times with double distilled water (DDW), and pH adjusted to 7-8. Finally, $NiFe_2O_4$ NPs were dried at 70 °C for 2 hrs.

2.2. Synthesis of the red emissive cationic carbon dots (rcCDs)

The rcCDs were synthesized as follows: 10 g of cetrimonium bromide (CTAB) was dissolved in 100 mL DDW and heated at 180 °C for 6 h. Boiled DDW was added when the solution was very low. Finally, the yellow rcCDs solution was dialyzed using a dialysis bag to remove the unreacted components.

2.3. General procedures for the proposed VA-D-μ-SPE method

50.0 mg of $NiFe_2O_4$ NPs were added to 10 mL of C2R solution (5-50 μM) and 10 mL of 0.5M phosphate buffer (pH 7.0), to achieve perfect C2R dye adsorption on $NiFe_2O_4$ NPs and vortexed for 20 min. Following the use of an external magnet to separate $NiFe_2O_4$ NPs from the solution mixture, the supernatant was decanted, and C2R was then released from the magnetic nanoparticles using 2 mL methanol and sonication for 5 min.

2.4. Colorimetric and fluorimetric sensing of C2R dye

The eluted solution containing C2R was measured colorimetrically at 510 nm after mixing with 1.0 mL of phosphate buffer (pH 7.0) and completing the volume to 10.0 mL with DDW. For the fluorimetric method, the eluted solution containing C2R was mixed with 2.0 mL of 300 µg.mL^{-1} rcCDs and 1.0 mL phosphate buffer (pH 7.0), followed by completion to 10.0 mL with DDW and incubation for 15 min. Colorimetric and fluorimetric spectra were recorded at room temperature. Scheme 2. Shows the general steps for the proposed methodology, where step I shows the VA-D-µ-SPE method while step II shows the synthesis of the fluorescent rcCDs for the fluorometric determination of C2R.

Scheme2. General steps for the proposed methodology, step I shows the VA-D-µ-SPE method while step II shows the synthesis of the fluorescent rcCDs and fluorometric determination of C2R via static and IFE quenching mechanism.

3. Results and discussion

3.1. Characterization of $NiFe_2O_4$ NPs

EDX analysis was used to determine the elemental composition of $NiFe_2O_4$ NP, as shown in Fig. 1a. O, Fe, and Ni elements are mainly observed in the $NiFe_2O_4$ NPs. The main functional groups of the as-prepared $NiFe_2O_4$ NPs were investigated using the FT-IR technique. Fig. 1b shows the FT-IR spectrum of the $NiFe_2O_4$ NPs, which is characterized by three distinct bands at 3370, 1625, and 655 cm^{-1}, respectively, corresponding to υ (OH), υ (C=O) (attributed to physically adsorbed surface moisture (O-H groups), and δ (Fe-O). The PXRD pattern of $NiFe_2O_4$ NP was investigated. Fig. 1c demonstrates the spinel structure of $NiFe_2O_4$ NPs with clear diffraction peaks at 31.4°, 36.4°, 40.8°, 43.9°, 54.8°, 58.8°, and 64.7°, respectively. These peaks correspond to the (220), (311), (222), (400), (422), (511), and (440) planes. These diffraction peaks are consistent with the standard $NiFe_2O_4$ (JCPDS no. 86-2267). SEM and TEM images of $NiFe_2O_4$ NPs are represented in Figs. 1d and 1e, respectively, where both the TEM and SEM images demonstrate spherical $NiFe_2O_4$ NPs with an average diameter of 20 nm. To evaluate the thermal behaviour and stability of $NiFe_2O_4$ NPs, the thermogravimetric analysis (TGA) was conducted at a constant thermal rate of 10 °C/min in the air atmosphere. As can be seen, the decomposition results of the $NiFe_2O_4$ NPs are observed in Fig. 1f. As presented, the TGA profile was characterized by 3 weight losses; the first mass reduction of $NiFe_2O_4$ NPs at the temperature range of 55–125 °C was nearly 21% and may be related to the elimination of surface adsorbed water. The maximum weight loss was observed in the range of 215–335 °C and was nearly 43%, which may be due to the initial breakdown of complexes and spontaneous combustion of reactants. The third weight loss was observed in the range of 385–475 °C and was nearly 20%, which may be due to further decomposition of organic impurities and the formation of oxide. Magnetic properties are measured by a vibrating sample magnetometer (VSM). Fig. 1g of the $NiFe_2O_4$ NPs shows the magnetic hysteresis curves. The magnetization of the $NiFe_2O_4$ NPs is 75 Am^2/kg. Accordingly, $NiFe_2O_4$ NPs have a superparamagnetic behaviour.

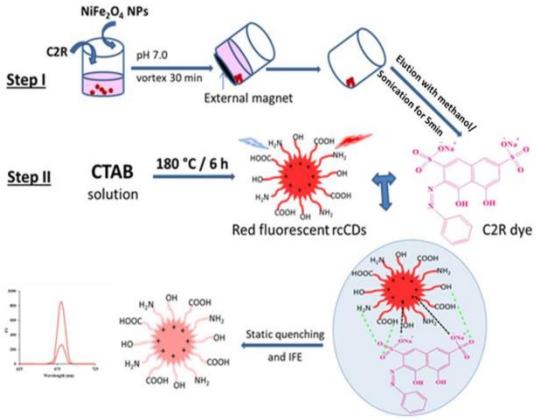

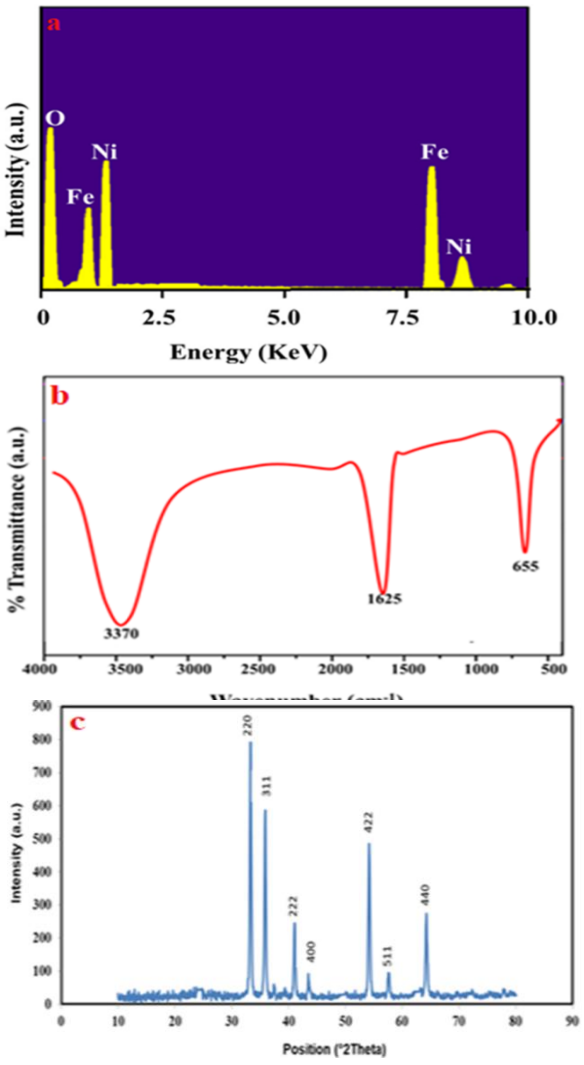

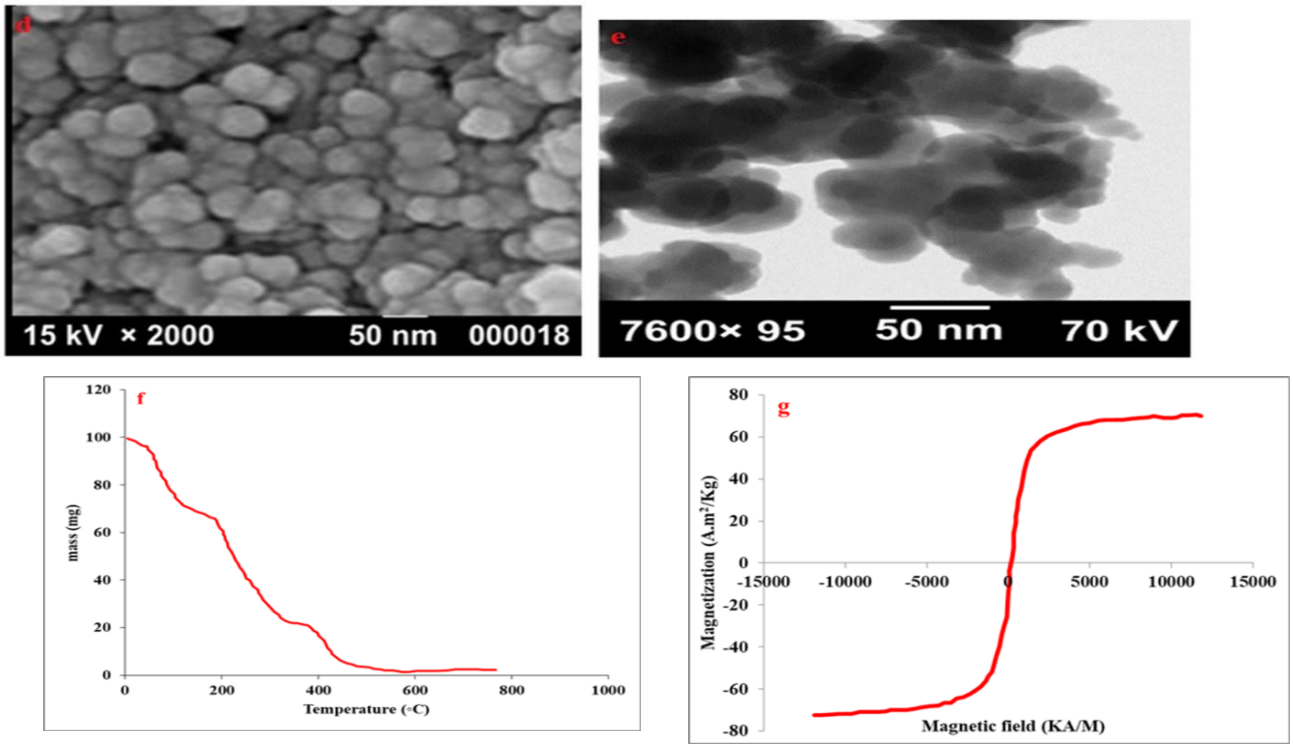

Fig. 1: EDX (a), FT-IR (b), and PXRD (c), SEM (d), TEM (e) images, TGA (f) and VSM (g) of $NiFe_2O_4$ NPs.

3.2. Characterization of rcCDs

The as-synthesized rcCDs displayed a noticeable excitation peak at 340 nm and a strong emission peak at 680 nm. Moreover, an absorption band of C2R was observed at λ_{max} of 510 nm (Fig. 2). The morphology of as-synthesized rcCDs was investigated using TEM images. Fig. 3a shows a spherical shaped and well dispersed rcCDs with a 3.4 nm average diameter. The FT-IR technique was used to investigate the rcCDs main functional groups. Fig. 3b shows the FT-IR spectrum of the rcCDs with four characteristic bands at 3350, 2800, 1710, 1635 cm^{-1}, 1205 cm^{-1}, which correspond to (OH, NH), (CH_2), (C=O, C=N), (N-H,OH), and (C-N), respectively, Moreover, the stability of rcCDs was studied under different conditions, including pH, temperature, and different ionic concentrations. In Fig. 3c, the as-fabricated rcCDs were found to be stable over a pH range of 6-10. In low pH mediums (pH 2 and 4), the high acidity causes protonation of the amine groups of rcCDs and produces ammonium conjugate acid, which is non-nucleophilic and makes the carboxylic groups on the surface of rcCDs after its carbonization in the unionized form, which decreases the fluorescence emission [40]. Moreover, the emission intensity of rcCDs was decreased by increasing the temperature, as shown in Fig. 3d, because increasing the temperature will speed up the molecular movement, leading to activated collisions and non-radiative emission, thereby decreasing the fluorescence emission. Furthermore, Fig. 3e shows that the emission intensity remained constant over a wide ranging of ionic concentration ranged from 0.1 to 2M concentration, suggesting that the as-synthesized rcCDs had excellent salt tolerance. The Quantum Yield (Φs) of the substance was determined by measuring it at λex of 340 nm. Quinine sulfate in a 0.10 M H_2SO_4 solution was used as a standard reference for comparison. The value of (Φs) was found to be 24.4%.

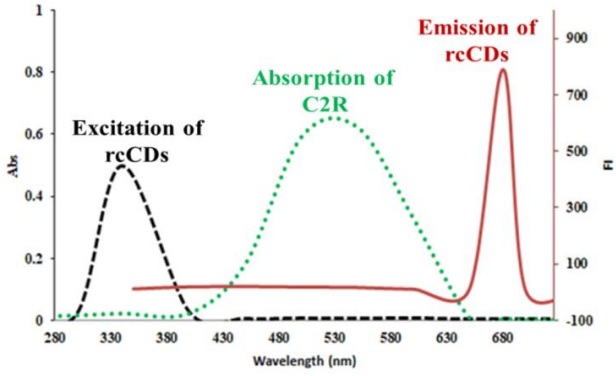

Fig. 2 Absorption spectrum of C2R dye; excitation and emission spectra of the rcCDs

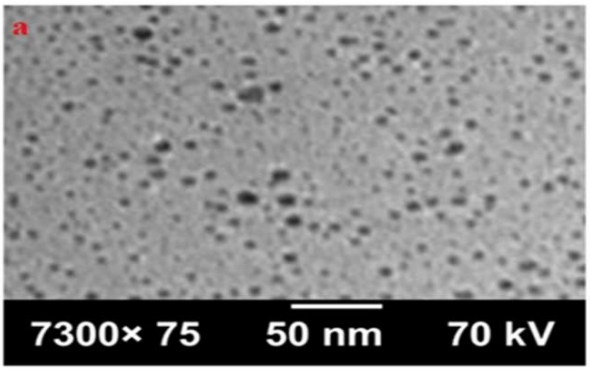

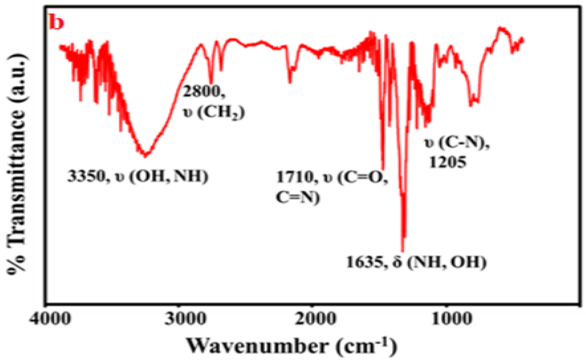

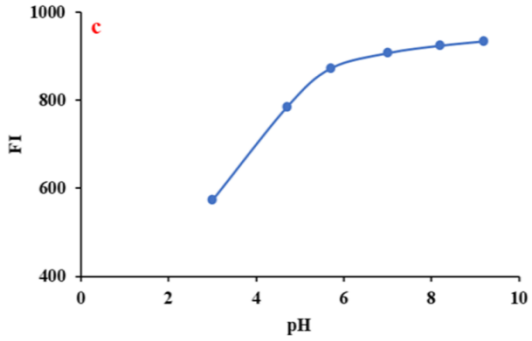

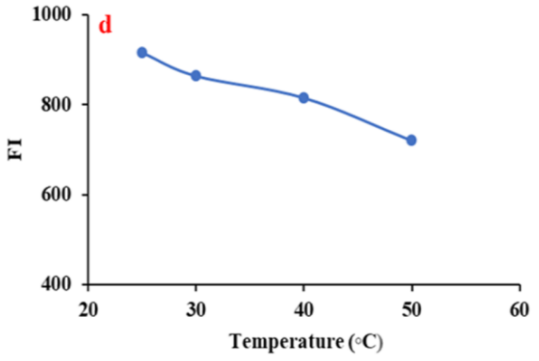

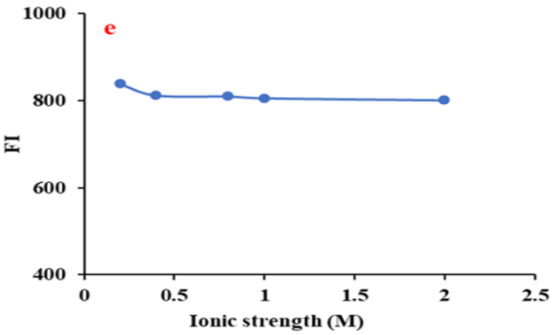

Fig. 3 TEM image (a) and FT-IR (b) of the rcCDs, fluorescence responses of rcCDs at different pH(c), different temperatures (d), and different concentration of ionic strengths (e).

3.3. Optimization of variables affecting determination and extraction

To get the highest possible sensitivity of the proposed method, we investigated and optimized the factors affecting the fluorescence intensity of rcCDs following their incubation with C2R dye, such as pH, incubation time, and diluting solvent (Fig. 4). It was found that the effect of pH was insignificant over a wide pH range (1.0-10.2), and decreased at pH values higher than pH 9.0. So pH 7.0 was used for the C2R assay. Furthermore, it was found that increasing the incubation time between the rcCDs and C2R resulted in more quenching, and stable readings were obtained after 15 min. Moreover, different diluting solvents were tested, such as DDW, ethanol, methanol, and tetrahydrofuran. It was found that the highest response was obtained with DDW, which may be attributed to the good dispersion and reaction of rcCDs.

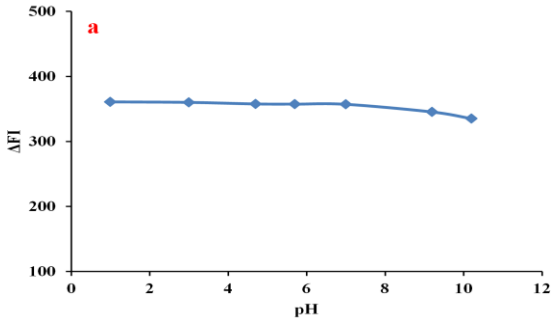

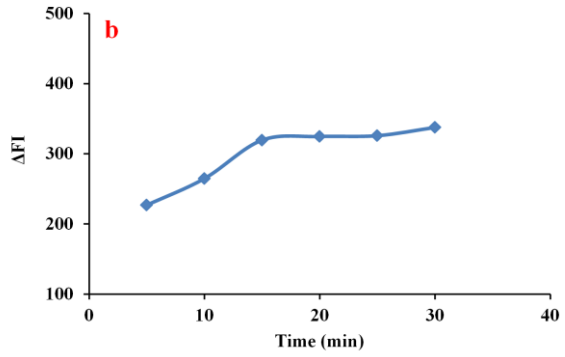

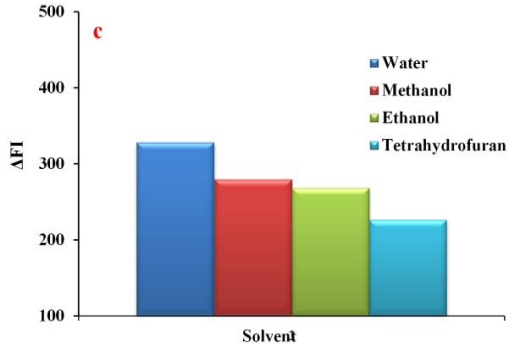

Fig. 4 The fluorescence intensity of rcCDs (300µg.mL^{-1}) after incubation with C2R dye (20 µM) at different pH (b), different incubation times (c), and different solvents (d).

3.4.1. Optimization of the VA-D-µ-SPE method

Fluorometric detection of C2R dye was used in optimization experiments of the variables because it is the main targeted methodology, while colorimetric detection of C2R dye was used in previous reports after its removal from aqueous samples using activated carbon [15]. To get the highest adsorption capacity, several factors affecting the adsorption of C2R on $NiFe_2O_4$ NPs were investigated and optimized, such as vortex time, $NiFe_2O_4$ NP amount, pH, C2R dye concentration, solvent, and ionic strength. Different amounts of $NiFe_2O_4$ NPs were tested (25, 50, 75, 100, 150, 200, and 250 mg) to attain the best amount of the adsorbent. The results showed that increasing the mass of $NiFe_2O_4$ NPs increased the adsorption until reaching 50 mg; after that, the adsorption remained constant. This is because there were more active sites for adsorption in the solution than free C2R molecules [41]. Therefore, 50 mg of $NiFe_2O_4$ NPs were chosen as the optimum amount, as shown in Fig. 5a. In addition, different pH values (in the range of 4.0-10.0) were investigated to attain the best pH suitable for the maximum adsorption of C2R on the $NiFe_2O_4$ NPs. The results showed a plateau of pH over the pH range 5.0-8.0, and therefore pH 7 was selected as the optimum pH as shown in Fig. 5b. This may be attributed to the fact that $NiFe_2O_4$ NPs have a zero point of charge near to pH=8 [42], which makes $NiFe_2O_4$ NPs positively charged at pH < 8.0 and facilitates their interaction with the negatively charged C2R in the aqueous solution. At pH > 8.0, the charges become negative on the $NiFe_2O_4$ NPs surface, resulting in repulsion between the $NiFe_2O_4$ NPs surface and the anionic C2R dye, decreasing the fluorescence signal. Moreover, the anionic C2R dye (due to its negatively charged SO_3^- groups) and the cationic rcCDs (positively charged) are maintained in the nearly neutral or slightly acidic aqueous solution, resulting in good electrostatic interaction and static fluorescence quenching [39]. Therefore, the adsorption experiments were conducted within the original pH of the solution. At pH < 4, protonation of C2R dye does not favour C2R adsorption as it may result in decreasing the electrostatic interaction between C2R and $NiFe_2O_4$ NPs adsorbent. Furthermore, Fig. 5c demonstrated that the maximum adsorption capacity was achieved after 20 min of vortex (contact) time followed by constant readings. As contact time increases, most sites are occupied, the adsorption effectiveness declines, and it is harder for the C2R dye to find a free sorption site [41]. 20 min was chosen as the optimum contact time. The ionic strength of the buffer solution can also affect C2R adsorption on the $NiFe_2O_4$ NPs because C2R is an anionic dye, and hence its adsorption on the $NiFe_2O_4$ NPs could be competitively influenced by the effect of salt ions on the available active adsorption sites. Therefore, a 0.5M phosphate buffer solution was used for further experiments, as shown in Fig. 5d. The effect of temperature on the adsorption of C2R dye on $NiFe_2O_4$ NPs was also studied using different temperature. Fig. 5e exhibited a decrease in ΔFI by increasing temperature, which may be due to destroying the adsorption bonds between the active sites in $NiFe_2O_4$ NPs and C2R dye. The enthalpy (ΔH) of C2R dye is negative (-7233.22 kJ/mol), indicating that the adsorption process is exothermic, and thus less C2R dye will be adsorbed at higher temperatures [42, 43].

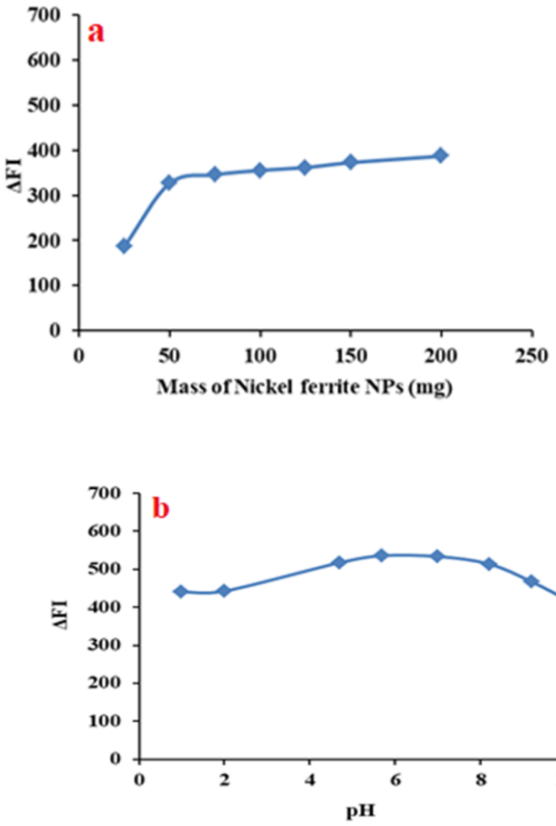

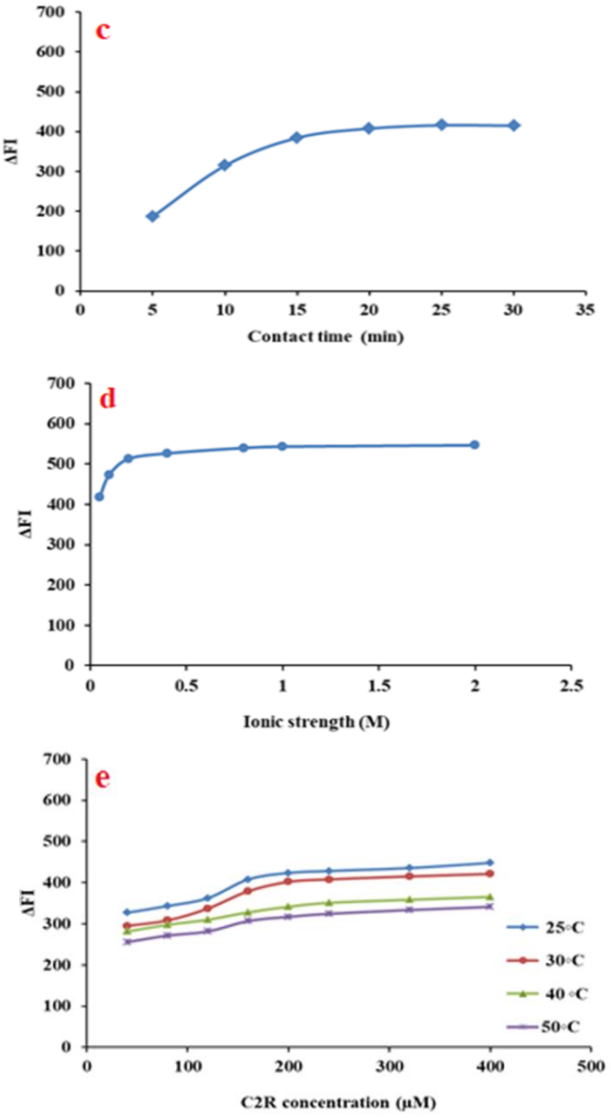

Fig. 5 Effect of (a) mass of the $NiFe_2O_4$ NPs, (b) pH, (c) vortex time, (d) ionic strength and (e) temperature on the adsorption of C2R dye (20 µM) after their incubation with $NiFe_2O_4$ NPs.

3.4.2. Mechanism of the fluorescence sensor

The structure of the anionic C2R dye carries a negative charge on its surface, while the cationic rcCDs are positively charged, which enables an electrostatic interaction resulting in fluorescence quenching. As well, according to the fluorescence and absorption spectra shown in Fig. 2, which show a small overlap in the spectral range between the absorption band of C2R dye and the emission and excitation spectra of rcCDs (although it is not at the λmax of absorption and emission/excitation), this suggests a quenching mechanism due to the inner-filter effect (IFE) [44]. To investigate the type of quenching mechanism of the rcCDs, if it is static or dynamic, the fluorescence ratio of the rcCDs in the presence and absence of series concentrations of C2R was measured at different temperatures (25, 30, 40, and 50 °C). The Stern-Volmer (SV) equation:

$$\frac{F^\circ}{F} = 1 + Ksv[Q] \ldots\ldots\ldots\ldots (4)$$

Where Ksv is the Stern-Volmer constant, $\frac{F^\circ}{F}$ is the ratio of fluorescence intensities, and Q is the quencher. The slope of the plot $\frac{F^\circ}{F}$ against $[Q]$ (Fig. 1S) at different temperatures was used to calculate the Ksv values. The results showed that Ksv values decreased (0.0376, 0.0244, 0.0142, and 0.0076) as the temperature increased (25, 30, 40, and 50 ˚C), respectively, which confirms the static quenching between C2R and rcCDs. Consequently, the fluorescence mechanism involved in this process can be attributed to both IFE and electrostatic quenching mechanisms.

3.5. Adsorption isotherms assessment

The Langmuir, Freundlich, and Temkin adsorption isotherm models were used to examine the C2R behaviour during its adsorption onto $NiFe_2O_4$ NPs [41]. To determine the highest adsorption capacity of $NiFe_2O_4$ NPs for C2R dye and to clarify the mechanism of the adsorption process, adsorption values were applied to the three adsorption models: Temkin (supposing adsorbent-adsorbate interaction), Langmuir (supposing identical adsorption venues), and Freundlich (supposing different adsorption venues). Construction of the Langmuir model based on the relationship;

$$\frac{Ce}{qe} = \frac{1}{kl\ qm} + \frac{Ce}{qm} \ldots\ldots\ldots (5)$$

Where qe, Ce, kl and qm are adsorbed quantity of C2R/g $NiFe_2O_4$ NPs at equilibrium, the C2R solution concentration at equilibrium, Langmuir equilibrium constant, and the ultimate adsorption capacity of $NiFe_2O_4$ NPs, respectively. Evaluation of this model relies on plotting $\frac{Ce}{qe}$ vs Ce (Fig. 2Sa) to gain a line having an intercept equal to ($\frac{1}{kl\ qm}$) and slope equal to ($\frac{1}{qm}$).

While Freundlich is based on the relationship[45];

$$qe = KfCe^{1/n} \ldots\ldots\ldots\ldots (6)$$

Where Kf and n are Freundlich constants. Evaluation of the Freundlich model based on plotting log q_e vs. log C_e (Fig. 2Sb) to attain a line having an intercept and slope equal to log K_F and 1/n, respectively. The affinity of C2R to $NiFe_2O_4$ NPs was evaluated by the (n) value [46]. Also, the Temkin model is constructed using relationships;

$$qe = BlnA + B\ lnCe \ldots\ldots\ldots (7)$$

Where (B) is a constant associated with heat of adsorption, and (A) is a constant utilized to investigate

$NiFe_2O_4$ NPs - C2R interaction. Evaluation of the Temkin model based on plotting (qe) vs. ($lnCe$) (Fig. 2Sc) to gain a line having an intercept and slope equal to ($BlnA$) and (B), respectively. Evaluation of the applied relationships depends principally on the correlation coefficient value, where the model with the highest R^2-value suggests the appropriate model for the adsorption process. The R^2 values shown in Table 1 indicate that the Freundlich model is the appropriate model for C2R dye adsorption on $NiFe_2O_4$ NPs. The q_e calculated was comparable with the obtained q_e from the experiment (2.34 $mg.g^{-1}$ and 50.72 $mg.g^{-1}$) respectively, because the *n*-values for the Freundlich model were much less than 10 and showed that C2R dye adsorption on $NiFe_2O_4$ NPs is heterogeneous, suggesting varying adsorption sites for C2R dye adsorption. When the R^2 values of the three isotherm models were compared, it was clear that the Freundlich model explained the adsorption of C2R onto the $NiFe_2O_4$ NP surface better. The *n* value derived from the Freundlich equation serves to describe the linearity of adsorption and ranges from 1 to 10 [46-48]. The resulted *n*-values ranged from 1.41-1.42, indicating a favorable biosorption process and adsorption sites [48].

Table 1 Parameters for Langmuir, Freundlich, and Temkin

Langmuir				Freundlich			Temkin		
T(◦C)	R^2	kl	qm	R^2	Kf	n	R^2	A	B
25	0.9708	0.0028	151.5	0.9958	9.0	1.4	0.8919	43.3	6.0564
30	0.9684	0.0026	149.2	0.9957	8.9	1.4	0.8919	43.4	6.0564
40	0.9726	0.0020	161.3	0.9957	8.9	1.4	0.8922	43.4	6.0567
50	0.9854	0.0024	133.3	0.9957	8.9	1.4	0.8920	43.3	6.0593

3.6. Investigation of thermodynamics of C2R adsorption

It is envisaged that hydrogen bonding would occur during C2R adsorption on $NiFe_2O_4$ NPs. So, it is anticipated that C2R adsorption onto $NiFe_2O_4$ NPs will be linked with a varying enthalpy (ΔH), entropy (ΔS) and free energy (ΔG) of the adsorption process. Thus, it was significant to estimate $\Delta Hads$ $_s$, $\Delta Sads$ and $\Delta Gads$ values. At optimized experimental conditions, ($\Delta Hads$) and ($\Delta Sads$) were calculated applying $\log\left(\frac{qe}{Ce}\right)$ vs. 1/T (Fig. 3S) via the following equations:

$$\log\left(\frac{qe}{Ce}\right) = \frac{\Delta Sads}{2.303R} - \frac{\Delta Hads}{2.303RT} \quad \text{..... (8)}$$

$$\Delta Gads = \Delta Hads - T\,\Delta Sads \quad \text{..... (9)}$$

Where R is the gas constant (8.314 $J.mol^{-1}$ Kelvin), and T is the absolute temperature (Kelvin). The C2R dye adsorption onto $NiFe_2O_4$ NPs is exothermic process according to the negative value (-7233.22 $KJ.mol^{-1}$) of ΔH^o. The positive value (35.06$J.mol^{-1}.K^{-1}$) of ΔS^o during the adsorption process showed decreased randomness at the solid-liquid interface. The results showed that (ΔG) values decreased (-3.2146, -3.3899, -3.7406, -4.0912 $KJ.mol^{-1}$) as the temperature increased (298, 303, 313, 323 K), suggesting spontaneous exothermic adsorption of C2R on $NiFe_2O_4$ NPs.

3.7. Evaluation of the adsorption kinetics

The adsorption rate and mechanism of C2R dye onto the $NiFe_2O_4$ NP surface were studied using the kinetic models: pseudo-first-order kinetic model (PFO) and pseudo-second-order kinetic model (PSO). Pseudo-first-order kinetic model equation:

$$\log(qe - qt) = logqe - \left[\frac{k1}{2.303}\right]t \text{..... (10)}$$

Pseudo-second-order kinetic model equation[49]:

$$\frac{t}{qt} = \frac{1}{k2qe2} + t/qe \text{..... (11)}$$

Where, $qe\ and\ qt$ equal amount of C2R is adsorbed at equilibrium time and time t, respectively ($mg.g^{-1}$). Table 3 shows the kinetic values of the investigated PFO and PSO models for the C2R adsorption onto $NiFe_2O_4$ NPs. The results showed that the R^2 value of the PFO model was 0.9197 and the difference between $qexp$ (experimental) and $qcal$ (calculated) was very large 2.34$mg.g^{-1}$ and 1.69$mg.g^{-1}$ respectively, so the PFO model did not fit the experimental data. On the other hand, the R^2 value of the PSO model was 0.9962, and the q_{exp} and q_{cal} values 2.34$mg.g^{-1}$ and 2.46$mg.g^{-1}$ respectively, were close to each other, indicating that the adsorption system followed the PSO model. The PSO constant ($k2$), and the adsorption equilibrium (qe) values were determined to be 6.830 $mg.min^{-1}$ and 2.46 $mg.g^{-1}$, respectively.

3.8. Comparison of C2R dye adsorption using different adsorbents

The study compared the C2R dye adsorption capability on various adsorbents based on the reported literature with that of the currently used $NiFe_2O_4$ NP. The adsorption capacity (q_m) served as the basis for this comparison. The results, presented in Table 2, showed that the qm value obtained in this study was greater than those reported in earlier works except for Activated carbon xerogels and Commercial activated carbon, which indicates the efficacy of the $NiFe_2O_4$ NP in eliminating C2R dye from aqueous solutions. This suggests that $NiFe_2O_4$ NP could be an effective adsorbent for future water treatment applications.

Table 2 Recent reported adsorption capacities of C2R dye

Adsorbent	Adsorption capacity q_m (mg.g^{-1})	Reference
Activated carbon xerogels	215.0	[50]
Commercial activated carbon	190.0	[51]
Activated carbon salvadora persica	20.4	[52]
Polyvinyl alcohol coated carbon salvadora persica	26.6	[52]
Graphene	108.5	[53]
Lanthanum mesoporous carbon	139.5	[54]
Aamla seed carbon	11.9	[51]
Tamarind seed carbon	5.0	[51]
$NiFe_2O_4$ NP	151.5	Present work

3.9. Validation of the proposed methods:

3.9.1. Linearity, LOQ and LOD

Under optimized conditions of the proposed VA-D-µ-SPE method, the emission intensity of rcCDs decreased as the amount of C2R dye increased due to fluorescence quenching of the rcCDs by C2R dye via the inner filter effect and static quenching. In the range of 5–50 µM, a plot of ΔFI vs. C2R concentration (Fig. 4S) revealed a linear connection with a determination coefficient (r^2) of 0.9993, a LOD (S/N=3) of 1.6 µM and LOQ (S/N= 10) of 5.5 µM. On the other hand, the absorption intensity of C2R increased linearly with increasing C2R concentration in the range of 10-60 µM with a LOD (S/N=3) of 3.1 µM and LOQ (S/N= 10) of 10.5 µM. The reproducibility of the proposed fluorimetric method was assessed by measuring the fluorescence quenching caused by 20 µM of C2R on the rcCDs emission intensity over three days. The results showed that the percentage relative standard deviation (% RSD) did not exceed 3.9%, indicating the fluorescence sensor's dependability for C2R determination. In terms of LOD, LOQ, and linear range, the proposed method was compared to the previously reported methods for determination of C2R dye. As shown in Table 3, the results showed that the proposed method is comparable to the reported methods.

Table 3 Comparison of analytical parameters with previously reported method of C2R dye

Method	Analytical parameters			Ref.
	LOD (µM)	LOQ (µM)	Linear range (µM)	
Spectrophotometric	11.5	38.0	10-298	[55]
Micellar electrokinetic chromatography	5-7.5	N/A	N/A	[56]
Extractive Spectrophotometric	4.9	16.0	6.5-382	[57]
Fluorimetric	1.6	5.5	5.0-50	Current study
Colorimetric	3.1	10.5	10.0-60	Current study

3.9.2. Real sample applications

In real samples, dual-fluorometric and colorimetric detection were used to demonstrate the advantages of the fluorometric method over the colorimetric method and to increase the reality of the analysis. To assess the suitability of the proposed VA-D-µ-SPE method with dual-mode fluorometric and colorimetric sensors, water C2R solutions were used as testing samples to determine C2R concentrations in these solutions in accordance with the optimized experimental procedure. The % recovery of the analysis was calculated using a standard addition method. Table 4 demonstrated that the obtained results were satisfactory, with the recovery percentage ranging from 92.6 to 102.4% and RSDs of not more than 3.5%. The recovery results indicated the good performance of the proposed VA-D-µ-SPE method for pre-concentration and extraction of C2R in real samples.

Table 4 The % recovery of C2R adsorption onto the $NiFe_2O_4$ NPs using the fluorometric and colorimetric sensors

Sample	Added (µM)	Measurements by colorimetric sensor	Measurements by fluorimetric sensor

		Found (µM)	% Recovery± SD	% RSD	Found (µM)	% Recovery± SD	% RSD
water	10	9.8	98.1±1.7	1.5	9.9	98.9±1.9	1.8
	20	20.5	102.4± 0.4	0.4	20.4	101.8± 3.6	3.5
	30	30.5	101.5±0.7	0.8	30.4	101.2+2.2	2.4
	40	39.8	99.4±1.4	1.3	39.9	99.7±1.8	1.7
	50	49.5	99.1± 1.1	1.1	49.7	99.4± 3.9	3.5
Tap water	10	9.9	98.9 ± 1.8	1.8	9.8	97.8 ± 1.6	1.5
	20	18.9	94.7 ± 0.9	0.9	19.1	95.3 ± 3.4	3.5
	30	28.4	94.6 ± 1.2	1.4	28.3	94.2 ± 1.4	1.6
	40	37.0	92.6 ± 2.1	2.2	37.6	93.9 ± 1.1	1.2
	50	48.7	97.4 ± 2.2	2.4	47.2	94.4± 3.9	1.4

The reusability of $NiFe_2O_4$ NPs for C2R adsorption was evaluated ($NiFe_2O_4$ NPs was washed three times with methanol and dried at room temperature before the next use): the $NiFe_2O_4$ NPs adsorbed 97% of C2R in the first cycle of the adsorption, whereas 93%, 87%, and 60% of C2R were adsorbed in the second, third, and fourth cycles, respectively. Therefore, the magnetic $NiFe_2O_4$ NPs are recyclable up to 3 times, displaying their stability during the application in water and tap-water analysis for C2R adsorption. This positive outcome offers a significant cost savings in the process of using $NiFe_2O_4$ NPs as C2R adsorbents in the water solutions.

4. Conclusion

Herein, a simple and cost-effective VA-D-µ-SPE using a dual-mode detection strategy was designed to concentrate and determine C2R in watery solutions. The approach relied on using $NiFe_2O_4$ NPs as solid- phase adsorbents for C2R, followed by dual-mode detection of C2R. The color mode is based on measuring the C2R absorbance at 510 nm, while the fluorimetric mode relies on quenching the emission of the as-synthesized rcCDs at 680 nm by C2R dye via the electrostatic interaction and the inner-filter effect. The suggested VA-D-µ-SPE method has both wider linear ranges and lower detection limits (LODs). This dual-mode solid-phase micro-extraction approach is environmentally friendly, inexpensive, and offers low LODs for C2R detection. Moreover, the studied adsorption kinetics and thermodynamics indicated that C2R adsorption onto $NiFe_2O_4$ NPs obeyed the Freundlich model, is considered a heterogeneous adsorption process with varying adsorption sites for C2R adsorption, and favores the PSO kinetic model.

Declarations

Ethics approval and consent to participate

Not applicable

Consent for publication

Not applicable

Availability of data and material

Not applicable

Competing interests

No potential conflict of interest was reported by the authors.

Funding

The authors declare that no funds, grants, or other support were received during the preparation of this manuscript

Authors Contributions

Conceptualization; formal analysis; investigation; methodology; data curation; software; validation; visualization; writing - original draft and editing by [Samer S. Aburub]. Proposal supervision; conceptualization; investigation; validation; and review by [Nurul Y. Rahim]. Conceptualization; methodology; investigation; field supervision; validation; visualization; review, and Data curation by [Ashraf M. Mahmoud].

References

[1] Robinson T, McMullan G, Marchant R, Nigam P. Remediation of dyes in textile effluent: a critical review on current treatment technologies with a proposed alternative. Bioresource technology. 2001;77(3):247-55.

[2] Netpradit S, Thiravetyan P, Towprayoon S. Adsorption of three azo reactive dyes by metal hydroxide sludge: effect of temperature, pH, and electrolytes. Journal of Colloid and Interface Science. 2004;270(2):255-61.

[3] Salleh MAM, Mahmoud DK, Karim WAWA, Idris A. Cationic and anionic dye adsorption by agricultural solid wastes: A comprehensive review. Desalination. 2011;280(1):1-13.

[4] Chen Q, He Q, Lv M, Xu Y, Yang H, Liu X, et al. Selective adsorption of cationic dyes by UiO-66-NH2. Applied Surface Science. 2015;327:77-85.

[5] Ashour HR, Ebrahiem EE, Mansour MS, Ghonim R. Application of nano adsorbent of PCMC in water treatment: removal of cationic dyes. Egyptian Journal of Chemistry. 2023.

[6] Pavithra KG, P SK, V J, P SR. Removal of colorants from wastewater: A review on sources and treatment strategies. Journal of Industrial and Engineering Chemistry. 2019;75:1-19.

[7] Rathi BS, Kumar PS, Vo D-VN. Critical review on hazardous pollutants in water environment: Occurrence, monitoring, fate, removal technologies and risk assessment. Science of The Total Environment. 2021;797:149134-.
[8] Samer S. Abu-Alrub MHM, Bandar A. A. Alyami, Ashraf M. Mahmoud, Yahya S. Alqahtani AOA. Development of spectrofluorometric method for determination of carmine dye (E120) in marketed juices products in Saudi Arabia. . Fresenius Environmental Bulletin. 2022;31(3):2576-9.
[9] Gita S, Hussan A, Choudhury TG. Impact of textile dyes waste on aquatic environments and its treatment. Environ Ecol. 2017;35(3C):2349-53.
[10] Molla A, Li Y, Mandal B, Kang SG, Hur SH, Chung JS. Selective adsorption of organic dyes on graphene oxide: Theoretical and experimental analysis. Applied Surface Science. 2019;464:170-7.
[11] Alaraby R, El Sayed MM. Methylene Blue Cationic Dye Removal using AA-Am Hydrogel as An Efficient Adsorbent. Egyptian Journal of Chemistry. 2022;65(12):1-10.
[12] Tan KB, Vakili M, Horri BA, Poh PE, Abdullah AZ, Salamatinia B. Adsorption of dyes by nanomaterials: recent developments and adsorption mechanisms. Separation and Purification Technology. 2015;150:229-42.
[13] Parmar M, Phutela UG. Biocolors: the new generation additives. Int J Curr Microbiol Appl Sci. 2015;4(7):688-94.
[14] Downham A, Collins P. Colouring our foods in the last and next millennium. International Journal of Food Science and Technology. 2000;35(1):5-22.
[15] Shahul Hameed K, Muthirulan P, Meenakshi Sundaram M. Adsorption of chromotrope dye onto activated carbons obtained from the seeds of various plants: Equilibrium and kinetics studies. Arabian Journal of Chemistry. 2017;10:S2225-S33.
[16] Sibel Ozkurt BAKMKFEGK, Sevin B. Respiratory Symptoms and Pulmonary Functions of Workers Employed in Turkish Textile Dyeing Factories. Int J Environ Res Public Health. 2012;9(4):1068-76.
[17] Hussein A, Miklas S. Treatment of artificial wastewater containing two azo textile dyes by vertical-flow constructed wetlands. Environmental science and pollution research international. 2018;25(7):6870-89.
[18] Goscianska J, Ptaszkowska M, Pietrzak R. Equilibrium and kinetic studies of chromotrope 2R adsorption onto ordered mesoporous carbons modified with lanthanum. Chemical Engineering Journal. 2015;270:140-9.
[19] Ribeiro RS, Fathy NA, Attia AA, Silva AMT, Faria JL, Gomes HT. Activated carbon xerogels for the removal of the anionic azo dyes Orange II and Chromotrope 2R by adsorption and catalytic wet peroxide oxidation. Chemical Engineering Journal. 2012;195-196:112-21.
[20] Puntes VF, Krishnan KM, Alivisatos AP. Colloidal nanocrystal shape and size control: the case of cobalt. Science. 2001;291(5511):2115-7.
[21] Singh E, Meyyappan M, Nalwa HS. Flexible graphene-based wearable gas and chemical sensors. ACS applied materials & interfaces. 2017;9(40):34544-86.
[22] Jiang Y-Q, Lu M-W, Huang X-H, Yang S-P, Tang Q. Controllable Magnetoresistance Device Based on a δ-Doped Magnetic Nanostructure. Journal of Nanoelectronics and Optoelectronics. 2016;11(4):523-8.
[23] Liu J, Huang C, He Q. Pharmaceutical application of magnetic iron oxide nanoparticles. Science of Advanced Materials. 2015;7(4):672-85.
[24] Wang C, Chen F, Chen Z, Liu C, Qian J, Wu Z, et al. Facile Synthesis of Ordered Mesoporous Cerium Oxide with Outstanding Catalytic Activity. Science of Advanced Materials. 2016;8(9):1760-5.
[25] Panda SK, Aggarwal I, Kumar H, Prasad L, Kumar A, Sharma A, et al. Magnetite nanoparticles as sorbents for dye removal: a review. Environmental Chemistry Letters. 2021;19(3):2487-525.
[26] El-Wekil MM, Ali HRH, Marzouk AA, Ali R. Enhanced dispersive solid phase extraction assisted by cloud point strategy prior to fluorometric determination of anti-hepatitis C drug velpatasvir in pharmaceutical tablets and body fluids. RSC advances. 2018;8(24):13292-300.
[27] Mohamed FA, Khashaba PY, El-Wekil MM, Shahin RY. Fabrication of water compatible and biodegradable super-paramagnetic molecularly imprinted nanoparticles for selective separation of memantine from human serum prior to its quantification: An efficient and green pathway. International journal of biological macromolecules. 2019;140:140-8.
[28] Mohamed FA, Khashaba PY, El-Wekil MM, Shahin RY. Spectrodensitometric determination of rivastigmine after vortex assisted magnetic solid phase extraction. Microchemical Journal. 2019;147:764-74.
[29] El-Wekil MM, Mahmoud AM, Alkahtani SA, Marzouk AA, Ali R. A facile synthesis of 3D $NiFe_2O_4$ nanospheres anchored on a novel ionic liquid modified reduced graphene oxide for electrochemical sensing of ledipasvir: Application to human pharmacokinetic study. Biosensors and Bioelectronics. 2018;109:164-70.
[30] Sivakumar P, Ramesh R, Ramanand A, Ponnusamy S, Muthamizhchelvan C. Synthesis and characterization of nickel ferrite magnetic nanoparticles. Materials Research Bulletin. 2011;46(12):2208-11.
[31] Luo PG, Sahu S, Yang S-T, Sonkar SK, Wang J, Wang H, et al. Carbon “quantum” dots for optical bioimaging. Journal of Materials Chemistry B. 2013;1(16):2116-27.
[32] Lim SY, Shen W, Gao Z. Carbon quantum dots and their applications. Chemical Society Reviews. 2015;44(1):362-81.
[33] Wang Y, Hu A. Carbon quantum dots: synthesis, properties and applications. Journal of Materials Chemistry C. 2014;2(34):6921-39.
[34] Hassan M, Gomes VG, Dehghani A, Ardekani SM.

Engineering carbon quantum dots for photomediated theranostics. Nano Research. 2018;11(1):1-41.
[35] Wang R, Lu K-Q, Tang Z-R, Xu Y-J. Recent progress in carbon quantum dots: synthesis, properties and applications in photocatalysis. Journal of Materials Chemistry A. 2017;5(8):3717-34.
[36] Yuan F, Li S, Fan Z, Meng X, Fan L, Yang S. Shining carbon dots: Synthesis and biomedical and optoelectronic applications. Nano Today. 2016;11(5):565-86.
[37] Yang W, Ni J, Luo F, Weng W, Wei Q, Lin Z, et al. Cationic carbon dots for modification-free detection of hyaluronidase via an electrostatic-controlled ratiometric fluorescence assay. Analytical Chemistry. 2017;89(16):8384-90.
[38] Namdari P, Negahdari B, Eatemadi A. Synthesis, properties and biomedical applications of carbon-based quantum dots: An updated review. Biomedicine & pharmacotherapy. 2017;87:209-22.
[39] Alyami BA, Mahmoud AM, Alkahtani SA, El-Wekil MM. $NiFe_2O_4$ nanospheres functionalized with 2-(2, 4-dihydroxyphenyl)-3, 5, 7-trihydroxychromen-4-one for selective solid-phase microextraction of aluminium. Talanta. 2021;226:122167-.
[40] Saberi Z, Rezaei B, Ensafi AA. Fluorometric label-free aptasensor for detection of the pesticide acetamiprid by using cationic carbon dots prepared with cetrimonium bromide. Microchimica Acta. 2019;186:1-7.
[41] Rozi SKM, Zulkifle AAM, Ishak AR, Rasdi FLM, Dom NC, Rahim NY, et al. Eggshell Membrane Functionalized with Waste Palm Cooking Oil for Removal of Alizarin Red from Aqueous Solutions. Malaysian Journal of Chemistry. 2022;24(2):12-23.
[42] Arora A, Gupta D, Rastogi D, Gulrajani ML. Kinetics and thermodynamics of dye extracted from Arnebia nobilis Rech. f. on wool. NISCAIR-CSIR. 2012;37(2):178-82.
[43] Bhatnagar A, Jain AK. A comparative adsorption study with different industrial wastes as adsorbents for the removal of cationic dyes from water. Journal of Colloid and Interface Science. 2005;281(1):49-55.
[44] Mahmoud AM, Mahnashi MH, Abu-Alrub SS, Alkahtani SA, El-Wekil MM. Indirect Differential Pulse Voltammetric Determination of Fluoride Ions at Carbon Paste Electrode Modified with Porous and Electroactive Fe 3+ /Fe 2+ Based-Metal Organic Frameworks Type MIL-101(Fe). Journal of The Electrochemical Society. 2021;168(12):126525-.
[45] Abobakr S, Abdo N. Adsorption Studies on Chromium Ion Removal from Aqueous Solution Using Magnetite Nanoparticles. Egyptian Journal of Chemistry. 2022;65(8):21-9.
[46] Özbay İ, Özdemir U, Özbay B, Veli S. Kinetic, thermodynamic, and equilibrium studies for adsorption of azo reactive dye onto a novel waste adsorbent: charcoal ash. Desalination and Water Treatment. 2013;51(31-33):6091-100.
[47] Anah L, Astrini N. Isotherm adsorption studies of Ni(II) ion removal from aqueous solutions by modified carboxymethyl cellulose hydrogel. Earth and Environmental Science. 2018;160:012017.
[48] Togue Kamga F. Modeling adsorption mechanism of paraquat onto Ayous (Triplochiton scleroxylon) wood sawdust. Applied Water Science. 2019;9(1):1.
[49] Mohamed S, Elshahat R. Accumulation of Iron, Zinc and Lead by Azolla pinnata and Lemna minor and activity in contaminated water. Egyptian Journal of Chemistry. 2021;64(9):5017-30.
[50] Ribeiro RS, Fathy NA, Attia AA, Silva AM, Faria JL, Gomes HTJCEJ. Activated carbon xerogels for the removal of the anionic azo dyes Orange II and Chromotrope 2R by adsorption and catalytic wet peroxide oxidation. 2012;195:112-21.
[51] Hameed KS, Muthirulan P, Sundaram MMJAJoC. Adsorption of chromotrope dye onto activated carbons obtained from the seeds of various plants: equilibrium and kinetics studies. 2017;10:S2225-S33.
[52] Daga K, Chaudhary S, Pallavi V. Removal of the Dye Chromotrope 2R Using Activated Carbon Prepared fromSalvadora persica: Kinetic and Equilibrium Studies. Nature Environment and Pollution Technology. 2010;9(2):345-50.
[53] Azari A, Nabizadeh R, Nasseri S, Mahvi AH, Mesdaghinia ARJC. Comprehensive systematic review and meta-analysis of dyes adsorption by carbon-based adsorbent materials: Classification and analysis of last decade studies. 2020;250:126238.
[54] Goscianska J, Ptaszkowska M, Pietrzak RJCEJ. Equilibrium and kinetic studies of chromotrope 2R adsorption onto ordered mesoporous carbons modified with lanthanum. 2015;270:140-9.
[55] Shah SN, Erbas Z, Soylak M. A novel-easy deep eutectic solvent-based microextraction procedure for the separation, preconcentration and spectrophotometric determination of chromotrope 2R in water, detergent and food samples. International Journal of Environmental Analytical Chemistry. 2022;102(14):3373-82.
[56] Desiderio C, Marra C, Fanali S. Quantitative analysis of synthetic dyes in lipstick by micellar electrokinetic capillary chromatography. Electrophoresis. 1998;19(8-9):1478-83.
[57] Okdeh M, Sakur AA, Alfares B. Extractive Spectrophotometric for Determination of Dihydroergocryptine Mesylate in Pharmaceutical Preparations. Asian Journal of Chemistry. 2014;26(10):2857.